



Modeling and Control of a Microgrid in Islanding Mode

F. Dulce¹, A. Gauthier² and A. Pantoja³

^{1,2} Departamento de Ingeniería Eléctrica y Electrónica
Universidad de los Andes
Bogotá, Colombia

e-mail: fa.dulce10@uniandes.edu.co, agauthie@uniandes.edu.co

³ Departamento de Ingeniería Electrónica
Universidad de Nariño
Pasto, Colombia

e-mail: ad_pantoja@udenar.edu.co

Abstract. Recent researches show the importance of modeling and control the DC/DC and DC/AC power converters in order to obtain proper-islanded microgrids or safe connection of different generation sources to the utility grid. The control needs arise because the high penetration of the low scale generation may produce frequency and voltage deviations from desired levels. In this context, this paper develops a model of distinct power converters and proposes a decentralized control strategy to regulate the frequency and voltage in a microgrid with different generators and loads. Simulations show the application of the control strategy in a simple microgrid model with the evaluation of every control stage in the grid.

Key words

Decentralized control, MPPT control, power converters, distributed generation, frequency and voltage regulation.

1. Introduction

Interconnected microgrids must coordinate distributed generation sources (DGs) connected independently to the utility grid. The main characteristics of the microgrids, additional to the DGs penetration, are their structure and control capability and coordination [1]. These aspects are different if the microgrids are connected to the main grid or work in island.

When the microgrid operate in islanded mode, the main problem is the frequency and voltage regulation. Connected to the utility grid, the microgrid take frequency and voltage set points from the grid, guaranteeing stability in the

operation. However, in islanded mode, the network parameters must be controlled by using power electronics devices coupled to the available DGs, given that synchronous units are not common in microgrids [2], [3]. Some works solve this control problem with decentralized methods as in [2] and [4], where the generators and connection filters are modeled through of a space-state model. The first paper uses an H_∞ control in the generator responsible of voltage regulation and PI controllers for current regulation. The second paper is based in a decentralized scheme with a droop control application acting over inverters to control the voltage levels. On the other hand, in [19] a microgrid central controller solves an optimization problem by defining a potential function for each DG unit and obtaining the minimum, which corresponds to the control objective of the generation units. Taking advantage of the renewable energy resources has motivated the research about DC/DC converters, mainly to reach the maximum power point (MPPT) of the photovoltaic generators. For instance, [5] and [6] propose different methods to reach the MPPT. The first one is based on fuzzy control combined with a search algorithm so-called perturb and observe (P&O). This algorithm changes iteratively the duty cycle of the DC/DC converter until it achieves the maximum generation power. Otherwise, the second paper proposes a method to obtain the MPPT using sliding mode control (SMC) by developing a space-state model and analyzing the converter dynamics without considering the converter set point.

Inverters are necessary devices to adequate the connection of DGs to the main grid or couple the action of other generators. The authors in [7] propose a new three-phase inverter topology capable to reach high frequency commutation reducing the output filter size. Moreover, in [8] and [9], an analysis of the traditional three-phase inverter topology is presented, focusing in the suppression of the DC current injected to the utility grid and an adequate design of the LCL output filter.

This work proposes a novel method to reach the MPPT in photovoltaic generators using a model that allow the power converters to find the maximum power voltage. Besides, we present a decentralized strategy through current control in each generator's inverter by modeling each converter,

F. Dulce is with Departamento de Ingeniería Eléctrica y Electrónica, Universidad de los Andes, Bogotá, Colombia. E-mail: fa.dulce10@uniandes.edu.co.

A. Gauthier is with Departamento de Ingeniería Eléctrica y Electrónica, Universidad de los Andes, Bogotá, Colombia. E-mail: agauthie@uniandes.edu.co.

A. Pantoja is with Departamento de Electrónica, Universidad de Nariño, Pasto, Colombia. E-mail: ad_pantoja@udenar.edu.co. This work has been supported in part by ALTERNAR Project, BPIN 20130001000089, Acuerdo 005 de 2013, OCAD – Fondo de CTeI- SGR, Colombia.

from the source to the connection point (PCC), and applying lineal and nonlinear control methods. The main goal of designed control is to achieve voltage and frequency regulation over the load connected at PCC when the microgrid is operating in islanded mode using only local controllers about the subsystems.

2. Secondary Control

The secondary control solves the energy management problem in a microgrid connected to the utility grid. Instead, when the microgrid is operating in islanding mode, the control is in charge of the voltage and frequency regulation [10]. We present a decentralized control that provides the most possible autonomy for all DG units and avoids the implementation of a large and complex communication system to coordinate the entire microgrid.

A. Microgrid Basic Model

Figure 1 shows an islanded system composed by two DG units, which could be photovoltaic panels (PV), energy storage systems (ESS), and low power synchronous generators, among others. Each DG is connected at the PCC through of inverters and LCL filters that avoid faults due to possible differences in output voltages. A RLC load is used for simulation with step variations considering the generation limits. The LCL filter model is analyzed as in [2] and [4] for a microgrid with decentralized control.

The aim of the control system is to regulate frequency and voltage at the PCC of a microgrid in islanding mode only with local controllers used on each DG. From Figure 1, the linear dynamic model of the microgrid is defined by the matrices

$$A = \begin{bmatrix} -\frac{1}{RC} & \frac{1}{C} & 0 & -\frac{1}{C} & \frac{1}{C} & 0 \\ -\frac{1}{L_1} & -\frac{R_1}{L_1} & \frac{1}{L_1} & 0 & 0 & 0 \\ 0 & -\frac{1}{C_1} & 0 & 0 & 0 & 0 \\ \frac{1}{L} & 0 & 0 & -\frac{R_L}{L} & 0 & 0 \\ -\frac{1}{L_2} & 0 & 0 & 0 & -\frac{R_2}{L_2} & \frac{1}{L_2} \\ 0 & 0 & 0 & 0 & -\frac{1}{C_2} & 0 \end{bmatrix} \quad B = \begin{bmatrix} 0 & 0 \\ 0 & 0 \\ \frac{1}{C_1} & 0 \\ 0 & 0 \\ 0 & 0 \\ 0 & \frac{1}{C_2} \end{bmatrix} \quad C = \begin{bmatrix} 1 & 0 \\ 0 & 0 \\ 0 & 0 \\ 0 & 0 \\ 0 & 1 \\ 0 & 0 \end{bmatrix}$$

with state variables x_1 as the load voltage (V_{abc}), x_2 and x_5 are the output currents i_1 and i_2 , respectively, x_3 and x_6 are the voltages in capacitors C_1 and C_2 , and x_4 is the current through of load inductor. The inputs or control signals are given by U_1 (control of generator 1 (i_{u1})) and U_2 (control of generator 2 (i_{u2})). Finally, the parameters R , L , and C represent the resistance, inductor, and capacitor of the load, L_1 , C_1 and L_2 , C_2 are the output inductors and capacitors of generator 1 and 2, and R_1 and R_2 are the internal resistance of inductors L_1 and L_2 .

Taking into account that inputs are the currents supplied by inverters in each generator, and that PCC voltage and DG_2 output current i_2 are the model outputs, the system can further be represented by [2]

$$\begin{bmatrix} \dot{x}_{DG1} \\ \dot{x}_{DG2} \end{bmatrix} = \begin{bmatrix} A_1 & E_1 \\ E_2 & A_2 \end{bmatrix} \begin{bmatrix} x_{DG1} \\ x_{DG2} \end{bmatrix} + \begin{bmatrix} B_1 & 0 \\ 0 & B_2 \end{bmatrix} \begin{bmatrix} U_1 \\ U_2 \end{bmatrix} \quad (1)$$

$$\begin{bmatrix} y_{DG1} \\ y_{DG2} \end{bmatrix} = \begin{bmatrix} C_1 & 0 \\ 0 & C_2 \end{bmatrix} \begin{bmatrix} x_{DG1} \\ x_{DG2} \end{bmatrix} \quad (2)$$

where $x_{DG1} = [x_1 \ x_2 \ x_3 \ x_4]^T$, $x_{DG2} = [x_5 \ x_6]^T$. The space-state equations (1) and (2) form an interconnected composite system. An interesting characteristic of this system is that if it is controllable and observable for all parameters, then it is stabilizable by using only local controllers in each subsystem [2], [11]. Because of the linearity of the representation, this property can be extended to bigger systems with more generators connected at the PCC. The control for the state variables x_{DG1} must deal with frequency and voltage regulation at the microgrid PCC in islanding mode (i.e., 120 Vrms and 60 Hz). On the other hand, the control applied to x_{DG2} regulates the current that generator DG_2 supplies to the load.

B. Control in DG_1 and DG_2

To achieve the frequency and voltage regulation, we propose a model predictive control (MPC), whose discrete model (A_d , B_d) is obtained from equations (1) and (2) with a fixed sampling time. Hence, the optimization problem is

$$\min \sum_{k=1}^{H_p} \|r - x_{DG1}(k)\|_Q + \|U_1\|_R \quad (3)$$

s. t.

$$x(k+1) = A_d x_{DG1}(k) + B_d U_1(k) \quad (4)$$

$$0 < U_1 < 1 \quad (5)$$

The objective function (3) seeks to minimize the control input and reduce the stationary state error between reference and the output, weighted by R and Q , respectively. The system output can be the load voltage or the output current. Equation (4) restricts the future states ensuring that the prediction is coherent with the discrete system model. Finally, condition (5) restricts the normalized applied control signal, where 1 represent the maximum output current which depend on the capacity of each generator. The controller reference signal is given by r , and H_p is the prediction horizon.

A similar optimization problem is formulated for the system representing the dynamics of the second generator that regulates the current of the load. In this case, the control signal U_2 is obtained as result. Once the controller performs the optimization procedure, the obtained control inputs U_1 and U_2 are the set points to the three-phase inverters in charge of supplying the necessary currents for voltage regulation on the load. The control strategies for the intermediate power converters and inverters are described in the next section.

3. Control of the Power Conversion Stages

Each generator is modeled as a constant source connected to a three-phase inverter, which is connected to a LCL filter as it is shown in Figure 1. However, between the source and the inverter there are some power conversion stages that adapt the voltage and current signals to obtain a final 60 Hz sine-wave, and obtain the maximum power from the primary source. The control of these stages is usually so-called local or primary control [10], [12]. This section presents each power conversion stage.

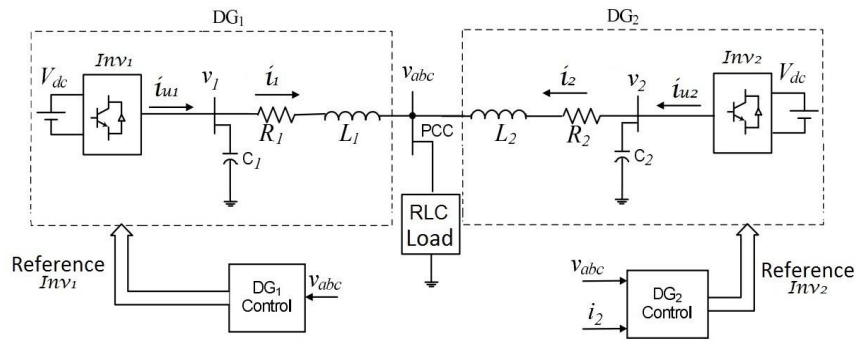


Figure 1 Islanding system scheme with tow generators connected in parallel. Adapted from [2]

A. Three-Phase Inverter

A three-phase-half-bridge inverter is used along with a LCL filter to obtain a low-harmonic sine-wave signal with $120V_{rms}$ and $60Hz$. This inverter is selected because of its simplicity and high performance [8], [9]. Each phase of the three-phase inverter is modeled independently in order to design only one controller to be replied in each line. The model to represent the dynamics of phase A, applying voltage and current Kirchoff laws is given by

$$\begin{aligned} \dot{x}_1 &= \frac{U}{L_a} - \frac{1}{L_a} x_2 \\ \dot{x}_2 &= \frac{1}{C_a} x_1 - \frac{1}{R_a C_a} x_2 \\ U &= \{V_1, -V_1\}, \end{aligned}$$

where V_1 is the inverter DC input voltage; L_a , C_a , and R_a are the inductor, capacitor, and resistance at the inverter output; x_1 is the current through inductor L_a ; x_2 is the voltage on capacitor C_a (output of the converter); and U is the on-off control signal for the switching devices of the inverter.

To get a sine-wave signal from a DC input, the inverter switches are activated to allow the change of the input voltage between V_1 and $-V_1$. The control aim is to obtain a $60Hz$ sine-wave output current with the set point given by the MPC described in the previous section. A sliding mode control (SMC) is used in this stage because of its discrete output. This method is widely used for systems with switching structure as the inverter. The SMC strategy is given by

$$\sigma(x) = K(x_1 - I_{ref}) + K_i \int (x_1 - I_{ref}) dt \quad (6)$$

$$U = \begin{cases} V_1 & \text{si } \sigma(x) < 0 \\ -V_1 & \text{si } \sigma(x) > 0 \end{cases} \quad (7)$$

where I_{ref} is the set point given for the secondary control (i.e., U_1 and U_2), K and K_i are constant to define a sliding surface $\sigma(x)$ (often so-called proportional and integral constants because of the equation (6) shape). To use an equivalent control method of sliding mode, first we determine the sliding surface $\sigma(x)$ that allow output current control. From Lyapunov analysis, the system stability is obtained when the inequality $KR_a > K_i(L_a - R_a^2 C_a)$ holds [13]. This condition determines the constants K and K_i , and the global stability is ensured selecting $K \gg 1$ and $0 < K_i < 1$. Finally, the applied input is determined by Equation (7).

B. Boost Converter

In order to provide a DC input signal to the inverter with the less possible variation, a DC/DC boost converter is proposed to obtain a continuous voltage signal despite of input variations. The model of a typical boost converter is presented in [18] and is given by

$$\begin{aligned} \dot{x}_1 &= \frac{E}{L} - \frac{U}{L} x_2 \\ \dot{x}_2 &= \frac{U}{C} x_1 - \frac{x_2}{RC} \end{aligned} \quad (8)$$

Where x_1 is the current through inductor L , x_2 is the voltage on capacitor C (output of the converter), E is the input voltage, L and C are the internal inductor and capacitor in the boost, R is the load resistor, and U is the control signal applied to a transistor with two possible states [18]:

$$U = \begin{cases} \text{transistor open} = 1 \\ \text{transistor close} = 0 \end{cases}$$

Given that the control goal is to maintain a constant input of $240V_{rms}$ in the inverter, we propose a simple state-feedback control with integrator to obtain the desired voltage from the boost converter. Due to the system in (8) is nonlinear and time-variant because of the change of E and R , the pole-placement strategy requires the linearization of the system for different operating conditions. In this case, variations of E are among $[1V \ 200V]$ and of R in $[2.4\Omega \ 1.2\Omega]$ are considered to emulate real loads. The final two dominant poles of the closed-loop system are chosen to obtain a fast response of the controller and null oscillations.

C. MPPT Control

The design of any generation system based on photovoltaic (PV) energy depends greatly of the maximum power point tracking (MPPT), due to the power supply depends on the operation voltage. The MPPT control allows the power converter to extract the maximum possible power of the generator at any operating condition for the incident solar irradiance and temperature over the photovoltaic modules.

1) *Model of a PV Generator:* a single-diode, shunt and series resistance gives a simple model of a PV cell. [18]. The equations that models the current variation in this circuit are given by [14], [15]:

$$I_m = I_{ph} - \left(\frac{I_{ph}}{A}\right) \left(e^{\frac{V_m + I_m R_s}{V_T}} - 1\right) \quad (9)$$

$$V_m = V_{oc} - I_m R_s - V_T \ln\left(\frac{V_m}{V_T} + 1\right)$$

where $A := e^{\frac{V_{oc}}{V_T}} - 1$, V_T is the thermodynamic voltage, R_s is the series resistance, I_{ph} is the photo-generated current, V_{mp} and I_{mp} are the voltage and current at peak power, and V_{oc} is the open circuit voltage.

Equation (9) allows us to calculate the current and voltage MPPT for different irradiance and temperature values [16], and obtain the voltage (V_m) that determines the point of maximum power. This voltage is used as reference for a SEPIC converter (Figure 2) to obtain the maximum energy extraction from PV generator.

2) *SEPIC Converter*: This converter has some advantages to achieve the MPPT in PV systems due to its non-inverted output voltage, low input current ripple, and high MPPT efficiency [6], [17]. The model of the converter shown in Figure 2 is given by

$$\begin{aligned} \dot{x}_1 &= \frac{I_{pv}}{C_i} - \frac{1}{C_i R_d} x_1 - \frac{1}{C_i} x_2 \\ \dot{x}_2 &= \frac{1}{L_1} x_1 - \frac{1}{L_1} x_3 - \frac{1}{L_1} x_5 \\ \dot{x}_3 &= \frac{U}{C_1} x_2 + \frac{1+U}{C_1} x_4 \\ \dot{x}_4 &= \frac{U}{L_2} x_5 - \frac{1-U}{L_2} x_3 \\ \dot{x}_5 &= \frac{U}{C_2} x_2 - \frac{U}{C_2} x_4 - \frac{1}{RC_2} x_5 \end{aligned} \quad (10)$$

Where x_1 and x_3 are the voltages in capacitors C_i and C_1 ; x_2 and x_4 are the currents through inductors L_1 and L_2 ; x_5 is the voltage in capacitor C_2 (converter output) C_i is the input capacitor; L_1, C_1, L_2 , and C_2 are internal inductors and capacitors, R is the PV internal resistance, I_{pv} is the PV current, and U is the control signal with two possible states:

$$U = \begin{cases} \text{transistor open} = 1 \\ \text{transistor close} = 0 \end{cases}$$

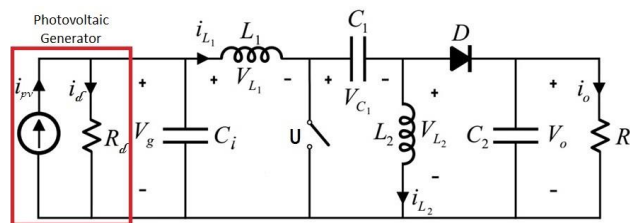


Figure 1 Scheme of a SEPIC converter coupled to a photovoltaic generator. Adapted from [6]

The model in Equation (10) represents the nonlinear dynamics of the SEPIC converter. Furthermore, these equations can be considered time-variant because of the changing value of I_{pv} according to the solar irradiance. The control objective is to reach the reference voltage (V_m) given by Equation (9) to extract the maximum power of PV generator. In this case, we propose the same state-feedback strategy used in the boost converter due to the similar characteristics of the models, with I_{pv} changing in the interval $[0.4A \quad 130A]$. An integrator is also aggregated to

the controller to obtain an asymptotic tracking without steady-state error.

In Figure 2, the PV source is modeled by using a Norton equivalent circuit, where the parameter R_d is the differential resistance of the source in its operating point and the current i_{pv} depends on the irradiance level and on the PV output voltage [6].

4. Simulations

A. Results

Figure 3 shows the simulation results for the secondary MPC control with load variations from 8 kW to 10 kW and then from 10 kW to 12 kW. In a), it is noticed that the voltage magnitude over the load maintains its value despite the load changes, providing asymptotic tracking with very low steady-state error. The decrease in voltage when the load increases is perceived, however, the stable state error remain in acceptable limits. The output PV current is shown in d), which is constant given that the incident irradiance and temperature are considered constant.

When the power increases from 8 kW to 10 kW, the current through the load increases from 31 A to 39 A (Figure 3 b)), because of the control over DG_2 . It keeps the output PV-current constant and the control over DG_1 allows an increase from 13 A to 21 A in the output current (Figure 3 c)). Given that DG_2 cannot supply more current because of the irradiance limit, the DG_1 have to supply the rest of the needed current. Thus, DG_1 must be dispatchable to avoid a collapse caused by load variations. In this sense, DG_1 is in charge of load voltage regulation. The simulation is performed with a synchronous generator of 20 kW and a PV generator of 5 kWp.

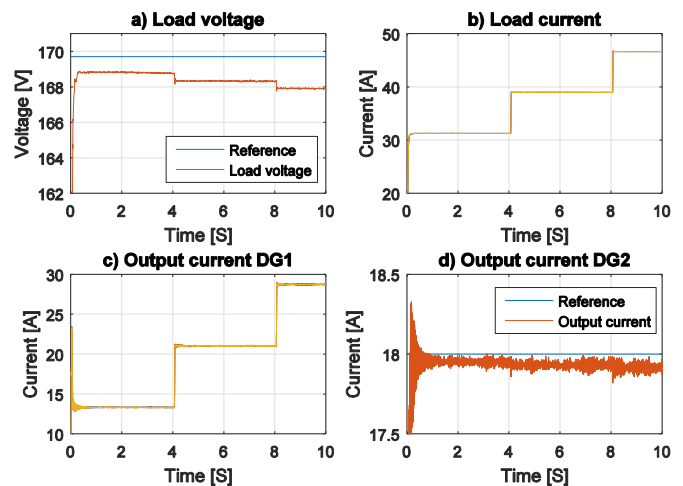


Figure 2 Response for the secondary decentralized control with two generators (DG_1 : diesel generator and DG_2 : PV generator)

Figure 4 a) shows the output voltage magnitude of the three-phase inverter with load variations from 1 kW to 6 kW in time intervals of 2 s. Due to the high frequency switching, the signal around the reference present an amplitude-limited noise. With higher switching frequency the harmonic distortion is reduced in the output. Besides, the noise presents a peak less than 1 V with a duration of less than 50 ms. In b), a close up is realized to the output inverter voltage at $t = 2$ s, where a load change occurs

from 1 kW to 2 kW. Note that the output signal has minimal error for the reference tracking and harmonic distortion. In c), it is observed that the output current increases when the load increases. However, the disturbance due to the load changes is low.

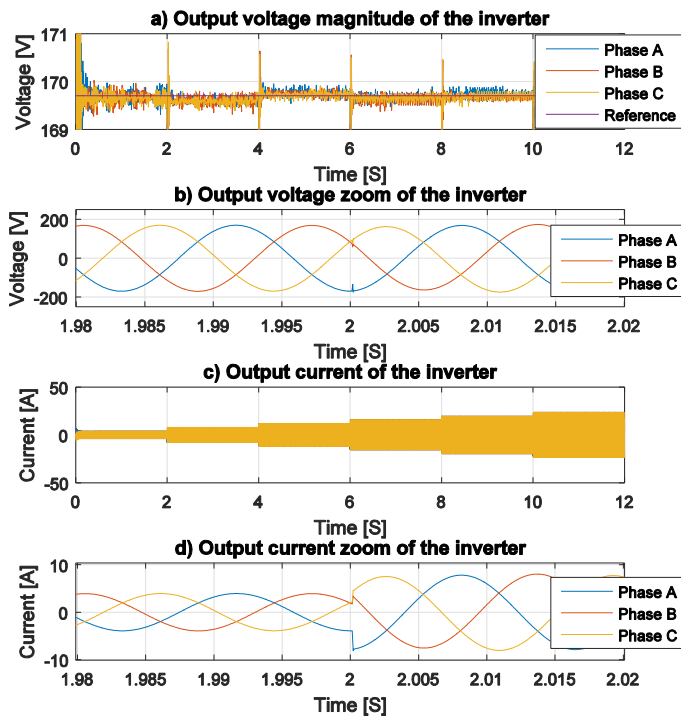


Figure 3 Responses to the control over the three-phase inverter

Figure 5 shows the simulation results for the DC/DC boost converter with voltage variations at the input in the shape shown in c), and the load variation presented in b). The first one represents the possible voltage variation due to irradiance changes and MPPT tracking, while the second one represents the load change that could occur at the output. In a), the controlled voltage is presented along with the reference signal. The controlled voltage has disturbances due to changes in the input voltage in steps of 10 V. However, the control is fast and effective to track the output to the reference value in less than 300 ms. It is possible to reduce the voltage peak produced by perturbations with a higher inductance in the output of the converter, trading-off with low settling times. Then, the disturbance recovery time is less than 1 s and the voltage peaks are not over 10 V, acceptable conditions for appropriate function of the system.

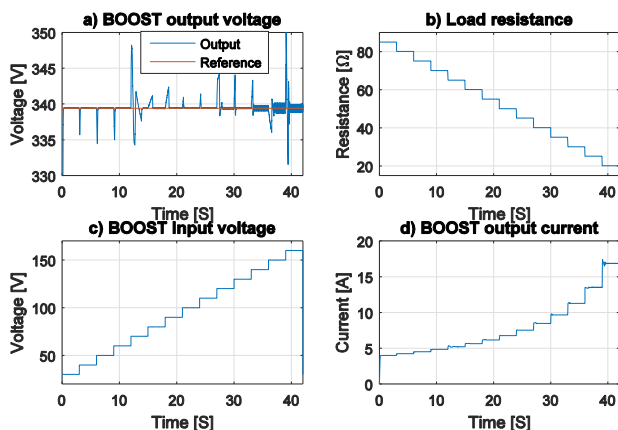


Figure 4 Voltage control in the BOOST converter

Figure 6 presents the control results for the SEPIC converter with irradiance variations from 100 W/m² until 1.2 kW/m² (Figure 6 e)) and ambient temperature among 15°C and 25 °C (Figure 6 f)). Figure 6 a) shows the MPPT voltage tracking, where the control tracks the reference given by the model in (9). However, the noise is also present in this case because of the high frequency switching in the converter. Nevertheless, it is possible to reduce noise in trade-off with speed of the response modifying the input capacitance C_i in the Figure 2. In this case a capacitor of 50 μF is selected to have a fast response and to maintain the commutation noise in a low level.

Figures 6 b) and c) represent the output current and the maximum power of the PV generator in function of the irradiance variation. The use of the model in (9) allows to achieve the MPPT taking as reference the information in the datasheet of the PV modules. In this case, a power peak of 5 kW can be obtained with an incident irradiance of 1 kW/m². Comparing b), c), and e) it is worth noticed that the power and current generated are proportional to the irradiance, contrary to the voltage in a). This is due to the physical properties of the PV modules based on semiconductors.

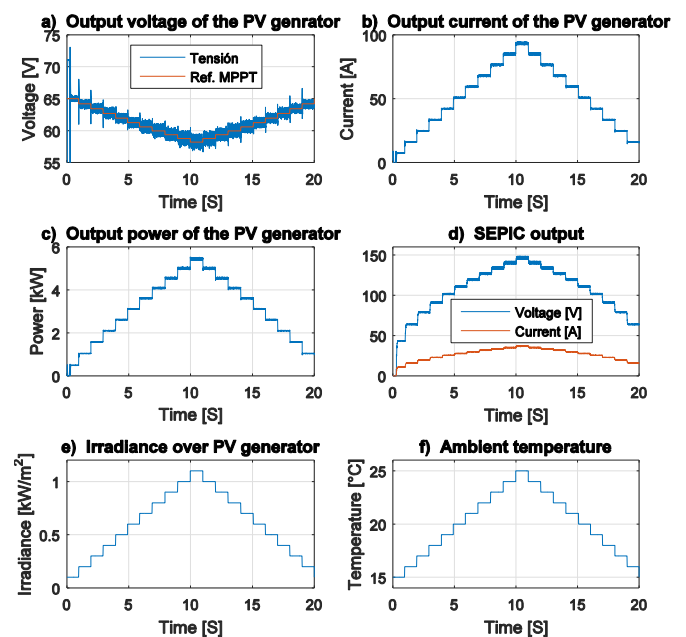


Figure 5 MPPT control in SEPIC converter

Figure 6 d) shows the change of the current and voltage at the SEPIC output. Comparing b), c) and d), it is clear that the output voltage is greater than the input voltage, while the output current is less than input current because of the control actions over the SEPIC converter. The controller regulates the input voltage as it is shown in a) and only one switch acts to perform the control action. Then, it is difficult to control both inputs and outputs at the same time. In consequence, the SEPIC output changes according to variation in the input, and for this reason a stable boost converter must be used to maintain a stable voltage at the inverter input.

5. Conclusion

In this work we propose a model to describe a microgrid composed by two distributed generators with possible extension to more units. Starting with analyzing the interconnection filter among generators, a state-space model is obtained, whose inputs are the output currents of the inverters. The application of a MPC control, the frequency and voltage levels at the load are maintained to expected levels.

Each generator is composed by a distributed source and power converters (i.e., two DC/DC converters and a three-phase inverter). A model is proposed along with the control of each converter. For PV generators, the MPPT control provides appropriate inputs to the inverter through a state-feedback control of the boost and SEPIC converters, guaranteeing also desired AC voltage levels over the load. Furthermore, the achieved MPPT points are verified by means of a PV model with real datasheet parameters.

References

- [1] N. Hatziaargyriou, *Microgrids Control Issues*, pp. 344–. Wiley-IEEE Press, 2014.
- [2] M. Babazadeh and H. Karimi, “Robust decentralized control for islanded operation of a microgrid,” in *2011 IEEE Power and Energy Society General Meeting*, pp. 1–8, July 2011.
- [3] N. Cai and J. Mitra, “A decentralized control architecture for a microgrid with power electronic interfaces,” in *North American Power Symposium (NAPS), 2010*, pp. 1–8, Sept 2010.
- [4] P. Li and P. Dou, “Power optimal decentralized coordinated control method of microgrid,” in *Power System Technology (POWERCON), 2014 International Conference on*, pp. 3010–3016, Oct 2014.
- [5] M. A. A. M. Zainuri, M. A. M. Radzi, A. C. Soh, and N. A. Rahim, “Development of adaptive perturb and observe-fuzzy control maximum power point tracking for photovoltaic boost dc-dc converter,” *IET Renewable Power Generation*, vol. 8, pp. 183–194, March 2014.
- [6] E. Mamarelis, G. Petrone, and G. Spagnuolo, “Design of a sliding-mode-controlled sepic for pv mppt applications,” *IEEE Transactions on Industrial Electronics*, vol. 61, pp. 3387–3398, July 2014.
- [7] M. A. Abusara and S. M. Sharkh, “Design and control of a gridconnected interleaved inverter,” *IEEE Transactions on Power Electronics*, vol. 28, pp. 748–764, Feb 2013.
- [8] E. Twining and D. G. Holmes, “Grid current regulation of a three-phase voltage source inverter with an lcl input filter,” *IEEE Transactions on Power Electronics*, vol. 18, pp. 888–895, May 2003.
- [9] T. Zhang, G. He, M. Chen, and D. Xu, “A novel control strategy to suppress dc current injection to the grid for three-phase pv inverter,” in *2014 International Power Electronics Conference (IPEC-Hiroshima 2014 - ECCE ASIA)*, pp. 485–492, May 2014.
- [10] S. Chowdhury and P. Crossley, *Microgrids and Active Distribution Networks*. Energy Engineering Series, Institution of Engineering and Technology, 2009.
- [11] E. Davison, “The robust decentralized control of a general servomechanism problem,” *IEEE Transactions on Automatic Control*, vol. 21, pp. 14–24, Feb 1976.
- [12] D. E. Olivares, A. Mehrizi-Sani, A. H. Etemadi, C. A. Cañizares, R. Iravani, M. Kazerani, A. H. Hajimiragha, O. Gomis-Bellmunt, M. Saeedifard, R. Palma-Behnke, G. A. Jiménez-Estévez, and N. D. Hatziaargyriou, “Trends in microgrid control,” *IEEE Transactions on Smart Grid*, vol. 5, pp. 1905–1919, July 2014.
- [13] J. Slotine and W. Li, *Applied Nonlinear Control*. Prentice Hall, 1991.
- [14] V. Quaschnig and R. Hanitsch, “Numerical simulation of current-voltage characteristics of photovoltaic systems with shaded solar cells,” *Solar Energy*, vol. 56, no. 6, pp. 513 – 520, 1996.
- [15] J. A. Gow and C. D. Manning, “Development of a photovoltaic array model for use in power-electronics simulation studies,” *IEE Proceedings - Electric Power Applications*, vol. 146, pp. 193–200, Mar 1999.
- [16] J. Hernández, *Metodología para el Análisis Técnico de la Masificación de Sistemas Fotovoltaicos como Opción de Generación Distribuida en Redes de Baja Tensión*. PhD thesis, Universidad Nacional de Colombia, Bogotá D.C., 2012.
- [17] S.-K. Chung, “A phase tracking system for three phase utility interface inverters,” *IEEE Transactions on Power Electronics*, vol. 15, pp. 431–438, May 2000.
- [18] L. Fialho, R. Melício, V.M.F. Mendes, A. Estanqueiro, “Simulation of a-Si PV system grid connected by boost and inverter”, *International Journal of Renewable Energy Research (IJRER)*, Vol. 5, N.º 1, pp. 443–451, 2015.
- [19] Sanjari, M. J., et al “Small signal stability based fuzzy potential function proposal for secondary frequency and voltage control of islanded microgrid.” *Electric Power Components and Systems*, Vol. 41, No. 5, pp. 485-499, 2013.